Contents lists available at ScienceDirect

# Biomedicine & Pharmacotherapy

journal homepage: www.elsevier.com/locate/biopha

# Docetaxel administered through a novel lymphatic drug delivery system (LDDS) improved treatment outcomes for lymph node metastasis

Ariunbuyan Sukhbaatar [a,b,c], Shiro Mori [a,b], Tsuyoshi Sugiura [a], Tetsuya Kodama [b,c,*]

[a] Division of Oral and Maxillofacial Oncology and Surgical Sciences, Graduate School of Dentistry, Tohoku University, 4-1 Seiryo, Aoba, Sendai, Miyagi 980-8575, Japan
[b] Laboratory of Biomedical Engineering for Cancer, Graduate School of Biomedical Engineering, Tohoku University, 4-1 Seiryo, Aoba, Sendai, Miyagi 980-8575, Japan
[c] Biomedical Engineering Cancer Research Center, Graduate School of Biomedical Engineering, Tohoku University, 4-1 Seiryo, Aoba, Sendai, Miyagi 980-8575, Japan

## ARTICLE INFO

## ABSTRACT

Recently, sentinel lymph nodes (LNs) have been recognized as a starting point of hematogenous metastasis; thus, an increase in the control rate of LN metastasis is expected to improve the survival rate. Although surgical treatment and radiation therapy are commonly used for the radical treatment of LNs, these treatments are associated with lymphedema, pain, and an extended hospital stay. In a recent mouse study, activation of metastatic tumors in distant organs was reported after removing LNs, with or without metastasis to the LNs. Thus, there is the necessity for cancer treatment that can replace LN removal. Here, we evaluated the treatment efficacy of lymphatic drug delivery system (LDDS) with osmotic pressure and viscosity escalated Docetaxel at the early stage of LN metastasis. MXH10/Mo/lpr mice were inoculated with mouse breast cancer cells into Subiliac LN to create the metastatic mouse model. Docetaxel was injected into mouse mammary carcinoma cells inoculated LN as a single shot (SS) or double shot (DS) to understand the therapeutic mechanism of a single shot or double shot intervention using an *in vivo* imaging system, histology, and qPCR. The results showed that the DS administration of docetaxel at 1,960 kPa (12 mPa•s) had better therapeutic outcomes with increased complete response and improved survival with reduced adverse events. The results also revealed that administration of a DS of docetaxel enhances differentiation of T helper cells, and improves survival and therapeutic outcomes. From a safety perspective, LDDS-administered DS of low-concentration docetaxel without any other anticancer treatments to LNs a novel approach to cancer management of LN metastasis. We emphasize that LDDS is a groundbreaking method of delivering anticancer drugs specifically to cancer susceptible LNs and is designed to enhance the effectiveness of cancer treatment while minimizing side effects.

## 1. Background

Lymph node (LN) metastasis has been identified in many cancer types and is associated with high aggressiveness, poor prognosis, and short survival times. Recently, sentinel LNs have been recognized as a starting point of hematogenous metastasis; thus, an increase in the

**Fig. 1.** A. Experimental design of MXH10/Mo/lpr mice studies that were inoculated with FM3A-Luc (19,800 cells/60 μL) into SiLN on day 0. Two DTX solutions with different osmotic pressure and viscosity, including ICG, were prepared: solution I (1,140 kPa, 4 mPa•s) and solution II (1,960 kPa, 12 mPa•s). Four DTX concentrations were prepared: 0.4 mg/node, 0.8 mg/node, 1.2 mg/node, and 1.6 mg/node. A single injection of DTX solution into ti-SiLN was administered on day 4, and double shots (DS) were administered on day 4 and day 8. B. Representative images showing ICG fluorescence intensity. C. Normalized fluorescence intensity change in ti-SiLN. AT: after treatment, BT: before treatment. The background level was normalized to the vertical axis before drug administration on day 4. D. Normalized fluorescence intensity change in PALN. The background level was normalized to the vertical axis before drug administration on day 4. AT: after treatment, BT: before treatment. E. Ex vivo fluorescence intensity in SiLN and PALN on day 42. Data are shown as the mean ± SEM (*$P \leq 0.05$, **$P \leq 0.01$, ***$P \leq 0.001$, ****$P \leq 0.0001$).

control rate of LN metastasis is expected to improve the survival rate. Although surgical treatment and radiation therapy are commonly used for the radical treatment of cancerous LNs [1], these treatments are associated with lymphedema, pain, and a long hospital stay. In a recent mouse study, activation of metastatic tumors in distant organs and LNs was reported after removing LNs, with or without metastasis [2–4]. Thus, there is the necessity for cancer treatment that can replace LN removal.

Metastasis to LNs begins with the invasion of tumor cells from afferent lymph vessels into the marginal sinuses [5]. LNs have well-developed vascular networks [6–9], and the branches (veins) extending from this vascular network anastomose with the veins running on the surface of the LNs [10]. Blood within the branches flows from inside the LN to outside [10]. Tumor cells growing in the marginal sinus of a LN may invade this branch in the early stages of proliferation and metastasize to distant organs through the blood stream [8,10,11], a metastatic concept termed the LN-mediated hematogenous metastasis theory. Other researchers have reported that LNs can be the starting point for remote points of cancer, as previously mentioned [12]. Tumor cells in the LNs receive oxygen and nutrients from this rich vascular network, $pO_2$ is constant [9], and they grow without inducing tumor neovascularization [13,14], replacing the parenchymal with tumor tissue, and structures such as a vascular network, high endothelial venules (HEVs), and notably the marginal sinuses disappear [15,16].

Tumor growth within the LNs also increases the internal pressure of LNs [17–19]. Therefore, it is assumed that conventional drug delivery methods through the vascular to target lymphatic systems [20] will have difficulty in maintaining sufficient drug concentrations in LNs or the lymphatic system in general in the early stages of metastasis, when either low-dose or high-dose anticancer agents are conventionally administered [20]. Recently, a lymphatic drug delivery system (LDDS) has been developed to deliver anticancer drugs directly to metastatic LNs [21–24]. This technique involves the administration of drugs directly into LNs under ultrasound guidance to treat the drug these LNs as well as secondary LNs located downstream in the lymphatic network. It is believed to be particularly effective for the therapeutic treatment of clinical N0 LNs [24].

In LDDS, solvents have an optimal osmotic pressure (700–3,000 kPa) and viscosity (<40 mPa·s) [25,26]. When hyperosmotic fluid is administered into LNs, blood components flow out from capillaries and high endothelial venules (HEV) of LNs and lymphatic channels occluded by tumor cells are dilated, while viscosity is considered to be related to drug retention [25,26]. These physicochemical parameters may increase the dilation of lymphatic channels and drug retention, which may promote passive diffusion of drugs into cells. The optimum conditions for osmotic pressure and viscosity may be achieved with most of the drugs currently used as systemic chemotherapy, drugs whose toxicity has halted further clinical trials, with synthetic micelles under development [27], dendrimers [28], inorganic nanoparticles [29] or liposomes [30].

Drug dose mg/m$^2$ scaling between species can be estimated based on the dose translation from human to animal studies [31] to assume systemic exposure of drugs administered systemically [32]. LDDS is one of the alternative routes, conventionally topical, intranasal, subcutaneous and intramuscular administration where the dose is limited by toxicities, but with LDDS the antitumor molecules are administered directly to the LNs at lower concentrations and significantly do not produce systemic toxicity. In the case of alternative routes of administration, the drug concentration at the site of administration should be translated between species. In the case of LDDS, if the dose is mg, then mg/node is the drug concentration at the site of administration. Sukhbaatar, et al. [25] administered docetaxel (DTX) (0.4 mg/node) to metastatic LNs of MXH10/Mo-*lpr/lpr* (MXH10/Mo/lpr) mice with enlarged LNs of the same size as human LNs (about 10 mm in diameter), and demonstrated the efficacy of LDDS. DTX is one of the most effective taxane-type anticancer drugs used for the treatment of recurrent primary tumor and LN metastasis in head and neck and breast cancer. For LDDS

administration the DTX solvent is adjusted to the optimum osmotic pressure and viscosity. Assuming that the size of lymph nodes in MXH10/Mo/lpr mice is equivalent to that in humans and that the amount of DTX per LN in mice is equivalent to the treatment of one LN in humans, the concentration per LN is 0.4 mg/node in mice and humans. Currently in clinical practice, the maximum dosage of DTX given systemic chemotherapy is 100 mg/m$^2$. Assuming a human body weight of 60 kg and a body surface area of 1.62 m$^2$ [33], this is 162 mg per body. Therefore, in LDDS, about 1/405 of the dose of systemic chemotherapy is administered to one metastatic lymph node. Successful completion of a phase 1 clinical trial of LDDS for head and cancer will require a defined dose per LN to determine the tolerability of the therapeutic agent and its pharmacodynamic and pharmacokinetic profiles. In the present study, DTX was dissolved in a solvent, with optimized osmotic pressure and viscosity, and given through the LDDS to determine the maximum recommended starting dose (MRSD) based on the therapeutic effect on metastatic LNs and the survival rate for the drug dose per LN.

## 2. Methods

### 2.1. Animal models

Animal experimental procedures were conducted in compliance with the Institutional Animal Care and Use Committee of Tohoku University's approved guidelines and the ARRIVE protocol. A recombinant inbred strain of mice, derived from MRL/Mp-*lpr/lpr* (MRL/lpr) and C3H/HeJ-*lpr/lpr*, MXH10/Mo-*lpr/lpr* (MXH10/Mo/lpr) mice (aged 12 – 16 weeks of age) [22,25,34,35] have enlarged peripheral lymph nodes (LNs) with a diameter of 10 mm, but crucially no severe autoimmune disease is induced unlike its ancestors. Mice were housed under specific pathogen-free conditions in the Animal Research Institute, Tohoku University. All experimental animal procedures were carried out under deep general anesthesia (2.5 % isoflurane in oxygen), and great care was taken to reduce animal suffering.

### 2.2. Cell culture

Stably-luciferase expressing murine mammary carcinoma cells (FM3A-Luc) [22,25,35] were cultured in RPMI-1640 medium (Sigma Chemical Co., St Louis, MO, USA) with the addition of 10 % (v/v) fetal bovine serum (Hyclone, GE Healthcare UK Ltd, Little Chalfont, UK), 1 % (v/v) L-glutamine-penicillin-streptomycin (Sigma) and 1 mg/mL G418 (Fuji Film Wako, Osaka, Japan). Cells were incubated at 37 °C in a 95 % air/5 % CO$_2$ atmosphere until 80 % confluence was achieved. The cells were passaged 3 to 4 times prior to inoculation into mice. Mycoplasma negativity was determined using a MycoAlert *Mycoplasma* Detection Kit (Lonza, Basel, Switzerland) on the day of inoculation.

### 2.3. Tumor cell preparation and inoculation into the SiLN

After 3 to 4 passages, mammary carcinoma cells were suspended in 20 μL of PBS plus 40 μL of Matrigel (400 mg/mL; Collaborative Biomedical Products, Bedford, MA, USA) to a final cell concentration of 19,800 cells/60 μL. After shaving and epilation were completed on a unilateral side of a mouse, the cell solution was inoculated into subiliac LN (SiLN; upstream LN, defined as the sentinel LN) to metastasize to the same side of the proper axillary LN (PALN; downstream LN of SiLN) to induce metastasis in the PALN (inoculation day was defined as day 0) (Fig. 1A). The tumor-inoculated SiLN (ti-SiLN) was irrigated with lukewarm saline (20 mL) and drained by using an M-20 aspirator (Tokyo M.I. Company, Inc., Tokyo, Japan) and the incision stitched with interrupted sutures (5–0 polyamide) (Neoblade N; Alfresa Pharma Inc., Osaka, Japan) to avoid infection after wound closure.

## 2.4. DTX preparation and injection

Two different DTX solutions of different osmotic pressures and viscosities were prepared: Solution I (1,140 kPa, 4 mPa·s) and Solution II (1,960 kPa, 12 mPa·s) [25]. All solutions consisted of DTX (80 mg/2 mL, DTX, Sanofi S.A, Paris, France, 0.5 mg/mL of indocyanine green (final concentration of 100 µg/mL, ICG, Daiichi-Sankyo Co., Tokyo, Japan), 100 % ethanol (Fuji Film Wako Pure Chemical Co, Osaka, Japan), polysorbate 80 (NOF Co., Tokyo, Japan), and distilled water and different concentration of DTX. No treatment was applied to the control group. 200 µL of DTX solution was injected into the ti-SiLN on day 4 for a single shot (SS) and on day 4 and day 8 for double shots (DS) at a bolus rate of 2,400 µL/min (Fig. 1A). The DTX concentration was 0.4 mg/node, 0.4 mg/node DS, 0.8 mg/node, 1.2 mg/node, 0.8 mg/node DS and 1.6 mg/node for Solution I and Solution II (the mouse body weight was assumed to be 40 g), and mice were randomly divided into an untreated or treated group.

## 2.5. Evaluation of treatment efficacy

Tumor growth or inhibition were tracked and noted using an in vivo bioluminescence imaging system (IVIS) based on luciferase expression of the FM3A-Luc cells on days 4 (before interjection), 8, 11, 18, 21, 28, 35 and 42 after tumor-inoculation, 10 min after intraperitoneal injection of 150 mg/kg luciferin (Promega, Madison, WI, USA). Luciferase activity around the ti-SiLN and PALN were measured on every experimental day and normalized to the luciferase activity reading on day 4 before treatment.

PALN metastasis was considered to have occurred when the luciferase activity exceeded the background level in controls ($1 \times 10^6$ photons/s). DTX retention and accumulation were measured using an in vivo biofluorescence imaging system (IVIS) on days 4 (before and after injection), 8, 11, 18, 21, 28, 35 and 42 after tumor-inoculation. Fluorescence intensity around the ti-SiLN (interjected site) and PALN were measured on every experimental day and normalized to the day 4 before treatment fluorescence intensity reading. On day 42 after tumor-inoculation, immediately after in vivo bioluminescence and biofluorescence measurements were taken, ti-SiLN and PALNs were excised and harvested, then ex vivo bioluminescence and biofluorescence were measured after mice were humanly euthanized.

## 2.6. Interactions between the DTX dose response

The response outcome of DTX dose dependence was evaluated using the Bliss independence model. Responses were measured as the percentage reduction in luciferase activity of cancer cells that died following injection of DTX; this measurement is referred to as the inhibition rate. The Bliss independence model was determined using equation ((1), $E_P$, predicted the combined effect; $E_A$ and $E_B$ individual effects with DTX) to establish interactions of DTX administration via LDDS (model constructed in the Excel module of Microsoft Office 365); data are presented as percentages $\pm$ SEM.

$$E_P = E_A \times E_B \tag{1}$$

Excess over Bliss score, difference between recited effect ($E_R$) and the Bliss predicted combined effect ($E_P$) at the same LDDS used to evaluate drug effects used the following criteria; >0, Synergism, = 0, Independent; <0 Antagonism.

## 2.7. Lymph node volume evaluation

ti-SiLN and PALN volumes were measured before inoculation, treatment and on every experimental day using a high-frequency ultrasound imaging system (VEVO770, FUJIFILM VisualSonics, Toronto, ON, Canada) with a 40 MHz transducer (RMV-704B; Visual Sonics). The step size between each B-mode slice was 0.1 mm, and the field of view was set to 15 mm × 15 mm. Values were normalized before inoculation to obtain normalized volume values.

## 2.8. Real-time qPCR for the immune profiling of dose dependency

To evaluate dose-dependent immune changes, a real-time quantitative polymerase chain reaction (qPCR) was performed as follows. DTX-treated tumor-inoculated mice were humanely killed 3 days after DTX dose initiation and the spleen, ti-SiLNs and PALNs were harvested, immersed in 5 volumes of *RNA*later (Sigma-Aldrich) overnight. Next, the mRNA was isolated using a FastGene Premium Kit (Nippon Genetics Co, Ltd., Toyo, Japan) according to the manufacturer's instructions. RNA sample purity and quality were verified using a Nanodrop 1,000 Spectrophotometer (Thermo Fisher Scientific, Massachusetts, USA) and quality and quantity verified (A260/280 > 1.8 and A 260/230 > 1.8) samples were synthesized for cDNA using a High-Capacity cDNA Reverse Transcription Kit and a RNase Inhibitor Kit (Applied Biosystems, California, USA). qPCR analysis was completed using TaqMan Gene Expression with ROX mixture (Thermo Fisher Scientific) by employing an AB7500 systems v2.3 (Applied Biosystems) to analyze spleen, ti-SiLN, and PALN mRNA gene expression of the following markers: pro-inflammatory cytokines (IL1-β, IL6, IL12-α, IL12-β, IFN-γ and TNF-α); tumor infiltrating lymphocytes (CD4, CD8, and PDL1); tumor suppressor (IL10 and TGF-β); and immunogenic cell death (Hsp70, Hsp90 and calreticulin). This was accomplished using pre-designed primers supplied by Integrated DNA (Supplementary Table S1). Data were normalized to an internal control (GAPDH) for each sample, and untreated and treated samples were compared with the main relative gene expression data.

## 2.9. Histological analysis

Excised ti-SiLN and PALN were excised on day 42 after tumor-inoculation and fixed for 4 days in 10% formalin, then dehydrated, embedded in paraffin, sectioned serially at 3 μm thicknesses and stained with Hematoxylin and Eosin (HE). The main histopathological findings were based on HE stained sections and images of the sections taken on a BX51 microscope (Olympus, Tokyo, Japan) or a digital slide scanner (NanoZoomer-SQ, Hamamatsu Photonics K.K., Hamamatsu, Japan). Tumor progression or treatment efficacy in the LNs were evaluated according to Supplementary Table S2. The designation of complete response (CR), partial response (PR), stable disease (SD) and progressive disease (PD) were on the basis of the standardized response definitions established by RECIST 1.1 criteria. CR was defined as the disappearance of all target lesions. Any pathological lymph nodes (whether target or non-target) must have had a reduction in the short axis to < 10 mm. PR was defined as at least a 30 % decrease in the sum of the diameter of target lesions, taking the baseline sum diameters as the reference. SD refers to a change of lesion size ranging from an increase of < 20 % to a decrease of < 30 % and with no new lesion. PD was defined as at least a 20 % increase in the sum of the diameters of target lesions, taking the smallest sum in the study as the reference.

## 2.10. Side effect evaluation

Dermatological, gastrointestinal, other possible side effects, or abnormalities that may be caused by DTX administration such as rash, alopecia, hematochezia, hematuria, and unusual motor skills were carefully documented. In addition, mice were weighed before inoculation and on every experimental day. However, no renal/hepatic toxicity was detected in previous LDDS experiments using CDDP [17,26], 5FU [24], doxorubicin [23] or DTX [25] 9 days after treatment. In the present study, blood biochemistry and hematology were evaluated 3 days after treatment. Briefly, blood was collected from IVC 3 days after treatment for the SS and DS groups of 1,960 kPa (12 mPa•s). A hematology test was conducted with Horiba Microsemi LC-662 using EDTA
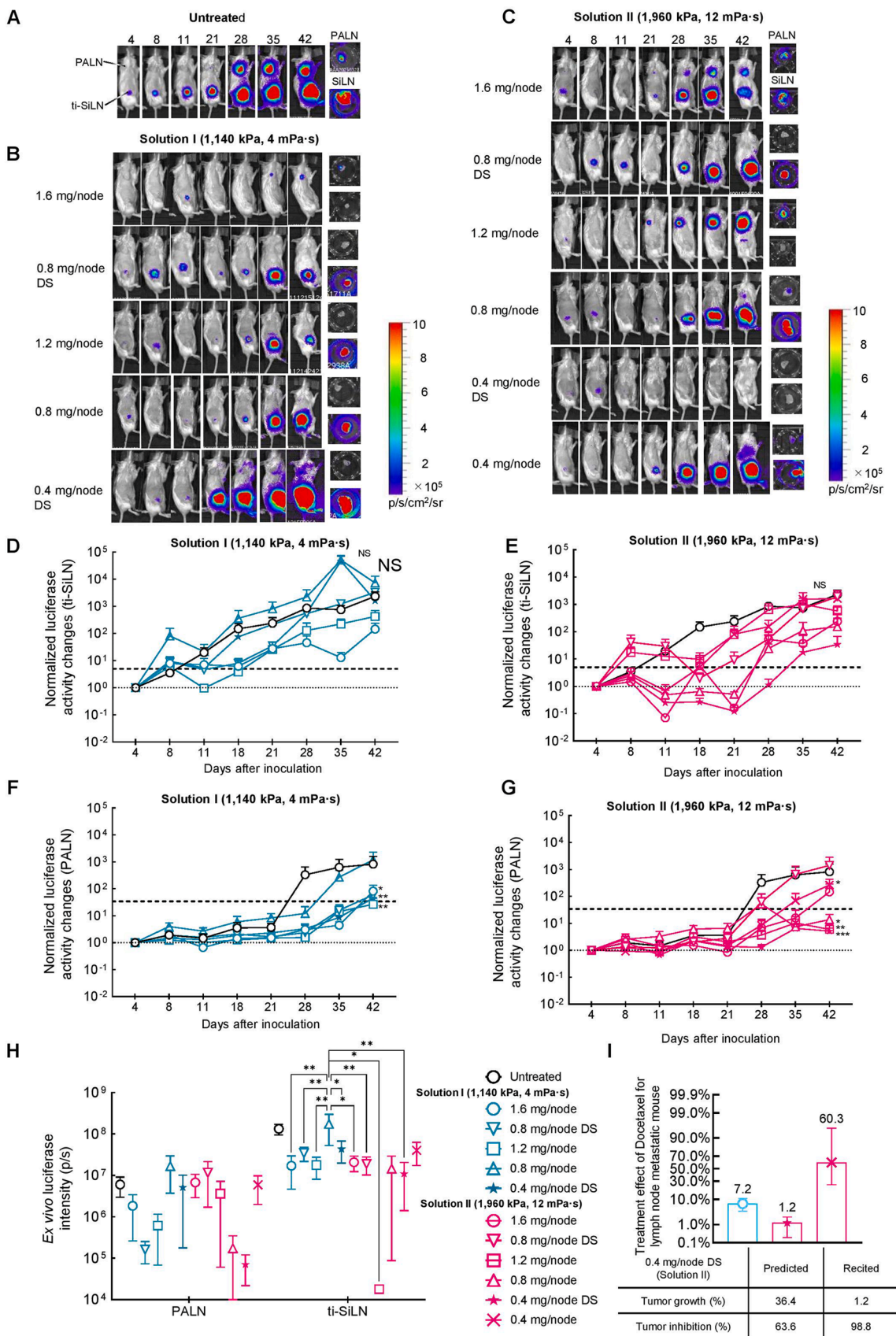
*(caption on next page)*

**Fig. 2.** Changes *in vivo* bioluminescence intensity over time after the administration of DTX using the LDDS. Untreated ($n = 8$); Solution I (1,140 kPa, 4 mPa·s). $n = 13 - 16$/group; Solution II (1,960 kPa, 12 mPa·s). $n = 4 - 9$/group. Data are shown as the mean ± SEM (* $P \le 0.05$, ** $P \le 0.01$, *** $P \le 0.001$, **** $P \le 0.0001$). A. Representative bioluminescence images showing luciferase activity. Untreated. B. Representative bioluminescence images showing luciferase activity. Solution I (1,140 kPa, 4 mPa·s). C. Representative bioluminescence images showing luciferase activity. Solution II (1,960 kPa, 12 mPa·s). D-G. Representative bioluminescence images showing luciferase activity. The luciferase activities were normalized to the value on day 4. Thin-dotted line (normalized at day 4), bold-dotted line (normalized by $1 \times 10^6$ photons/s). D. Solution I, ti-SiLN. E. Solution I, PALN. F. Solution II, ti-SiLN. G. Solution II, PALN. H. *Ex vivo* luminescence intensity in PALN and ti-SiLN was obtained on day 42. Data are shown as the mean ± SEM (* $P \le 0.05$, ** $P \le 0.01$, *** $P \le 0.001$, **** $P \le 0.0001$). I, Response outcome of DTX dose response evaluated by Bliss Independence. Tumor inhibition was 7.2 % for 1.6 mg/node of Solution I, 1.2 % for 0.4 mg/node DS (Solution II) and 60.3 % for 0.4 mg/node (Solution II).

treated whole blood whereas biochemistry tests were carried out using FujiFilm DriChem 7000 v (FujiFilim Veterinarian Kit) according to manufacturer's instructions. Histologically confirmed healthy 12-week-old MXH10/Mo/lpr blood samples were used for the baseline.

### 2.11. Verification of optimal range of osmotic pressure and viscosity using LDDS infused cisplatin (CDDP)

To verify the experimental technique and model, 16,000 cells/40 μL of KM-Luc/GFP cells suspended in a mixture of PBS and Matrigel were injected into the unilateral side of the PALN (tumor inoculated PALN, ti-PALN) of MXH10/Mo/lpr mice ($n = 6$). On day 3 after-inoculation, 1 mg/kg CDDP at increased osmotic pressure and viscosity was infused using the LDDS into the SiLN at the rate of 10 μL/min for 20 min to inhibit tumor growth in the ti-PALN. Flow dynamics of CDDP were measured using the biofluorescence imaging IVIS and side effects of a low rate of infusion were evaluated with VEVO770; and the treatment effect was confirmed by histology.

### 2.12. Statistical analysis

Data were analyzed with Excel and GraphPad Prism 8.4.3 (GraphPad Software, La Jolla, CA, USA) and the results are given as the mean ± standard error of the mean (S.E.M.) or standard deviation (S.D.). The Mann-Whitney test used to assess the significance of mRNA expression levels (mean ± S.E.M.). The 95 % CI for progression free survival (PFS) and overall survival (OS) analyses were noted, and the time to event and comparisons were performed using the Kaplan-Meier method and log-rank test, respectively. Throughout the two-way ANOVA and Tukey's post hoc test analyses, a two-sided *P*-value < 0.05 was considered to be a statistically significant finding.

## 3. Results

### 3.1. Evaluation of the prolonged treatment efficacy of LDDS-injected DTX (SS and DS)

In these experiments, experimental lymph node metastatic mice were used in which tumor cells were inoculated into the SiLNs [25]. A tumor-inoculated SiLN (ti-SiLN) was defined as the sentinel lymph node and the PALN as the downstream lymph node. DTX solutions (0.4–1.6 mg/node) (Solution I, Solution II) were administered to ti-SiLNs on day 4 for SS and on days 4 and 8 for DS after tumor inoculation, and the antitumor effects on the ti-SiLNs and PALNs were evaluated (Fig. 1A). The TDX solution contains ICG, and the flow dynamics of DTX solution in the body were evaluated by fluorescence intensity (Fig. 1B–D). Regardless of whether it was a SS or DS, immediately after the administration of DTX (AT: after treatment), ti-SiLN (Fig. 1C) flowed out to the PALN (Fig. 1D). Statistically significant differences in ti-SiLN and PALN retention were observed for each solution type and administration condition (Fig. 1D). In addition, cyclic increases and decreases in the retention intensity were observed on days 11, 18 and 35. Fig. 1E shows the fluorescence intensity in the ex vivo condition. Comparing Solution I and Solution II, the fluorescence intensity was higher in Solution I under the same administration conditions.

Next, the tumor growth inhibitory effect of DTX was evaluated

(Fig. 2). In the in vivo bioluminescence images, the growth of tumor cells in the ti-SiLN and metastatic PALN were observed over time (Fig. 2A). Administration of Solution I and Solution II to ti-SiLN suppressed tumor growth, in particular the antitumor effects of solution I (1.6 mg/node) (Fig. 2B) and solution II (0.4 mg/node DS) (Fig. 2C) were remarkable. Fig. 2D–G show the changes in luciferase activity over time. The dashed thin line is the dimensionless value of luciferase activity on day 4. The dashed thick line is the value obtained based on 1106 p/s, which was defined as the value at which the transition of metastasis into PALN was confirmed. Luciferase activity of ti-SiLN was suppressed up to day 18 (Fig. 2D), except for 0.4 mg/node and 0.8 mg/node in Solution I groups (Fig. 2D). Proliferation of tumor cells in the PALN inhibited the up to day 42 except for 0.8 mg/node (Fig. 2E) in Solution I groups. In solution II (Fig. 2F), tumor growth in the ti-SiLN was inhibited up to 0.4 mg/node until day 28 (Fig. 2F), and the tumor growth in PALN was inhibited at 0.4 mg/node and 0.8 mg/node up to day 42 (Fig. 2G). Ex vivo luciferase activity was measured on day 42 and statistically significant differences were found between Solution I and Solution II in the SiLN (Fig. 2H). The response outcome of DTX dose dependency was analyzed by Bliss independence and $E_P$ was 36.4 and $E_R$ 1.2 % in the 0.4 mg/node of the Solution II groups (Fig. 2I). Thus, the effects of a DS of Solution II treatment were synergistic.

### 3.2. Survival benefit of an LDDS-injected DTX dosage at high osmotic pressure and viscosity

Next, we examined the survival rate associated with LDDS injected DTX (Fig. 3, Table 1). Fig. 3A and B show the survival rates for Solution I and Solution II, respectively. In the untreated group, the survival rate was 63 %. The survival rates below this value were 0.8 mg/node (Solution I) (Fig. 3A) and 1.6 mg/node (Solution II) (Fig. 3B). The survival times of the mice were prolonged as drug concentration increased, but not the treatment efficacy. Fig. 3C–F shows the volume changes of the ti-SiLN and PALN, when both Solution I and Solution II suppressed the volume increase compared to the untreated group. Temporal volume increases were observed in the treated ti-SiLN due to drug retention in it, an indicator of edema (Fig. 3C, E). Solution II was more effective than Solution I in suppressing the volume increase. This effect depended on the concentration of DTX and the frequency of its administration per lymph node.

### 3.3. Post-mortem histopathological assessment

Fig. 4 shows the scoring results for the lymph nodes with *ex vivo* luciferase activity of excised ti-SiLNs and PALNs and histological evaluation (Fig. 5) of day 42 after tumor-inoculation, respectively. In the untreated group, the ti-SiLN was completely replaced with tumor cells, scoring 3 whereas 40 % of the PALNs had a score of 3 % and 60 % of LNs were occupied with tumor cells, with invasion in more than half of the LN (Fig. 4A and B). Better treatment efficacy was found for: ti-SiLN treatment at 1.2 mg/node, 0.4 mg/node, 1.6 mg/node of Solution I; 1.2 mg/node, 0.4 mg/node DS, 0.8 mg/node of Solution II. For PALNs, 1.2 mg/node, 0.8 mg/node DS, 0.8 mg/node of Solution I; 0.4 mg/node DS of Solution II (Fig. 4C). Overall, the best treatment efficacies based on ex vivo imaging and histology were found to be 1.6 mg/node of Solution I and 0.4 mg/node DS of Solution II, with consideration of severity of
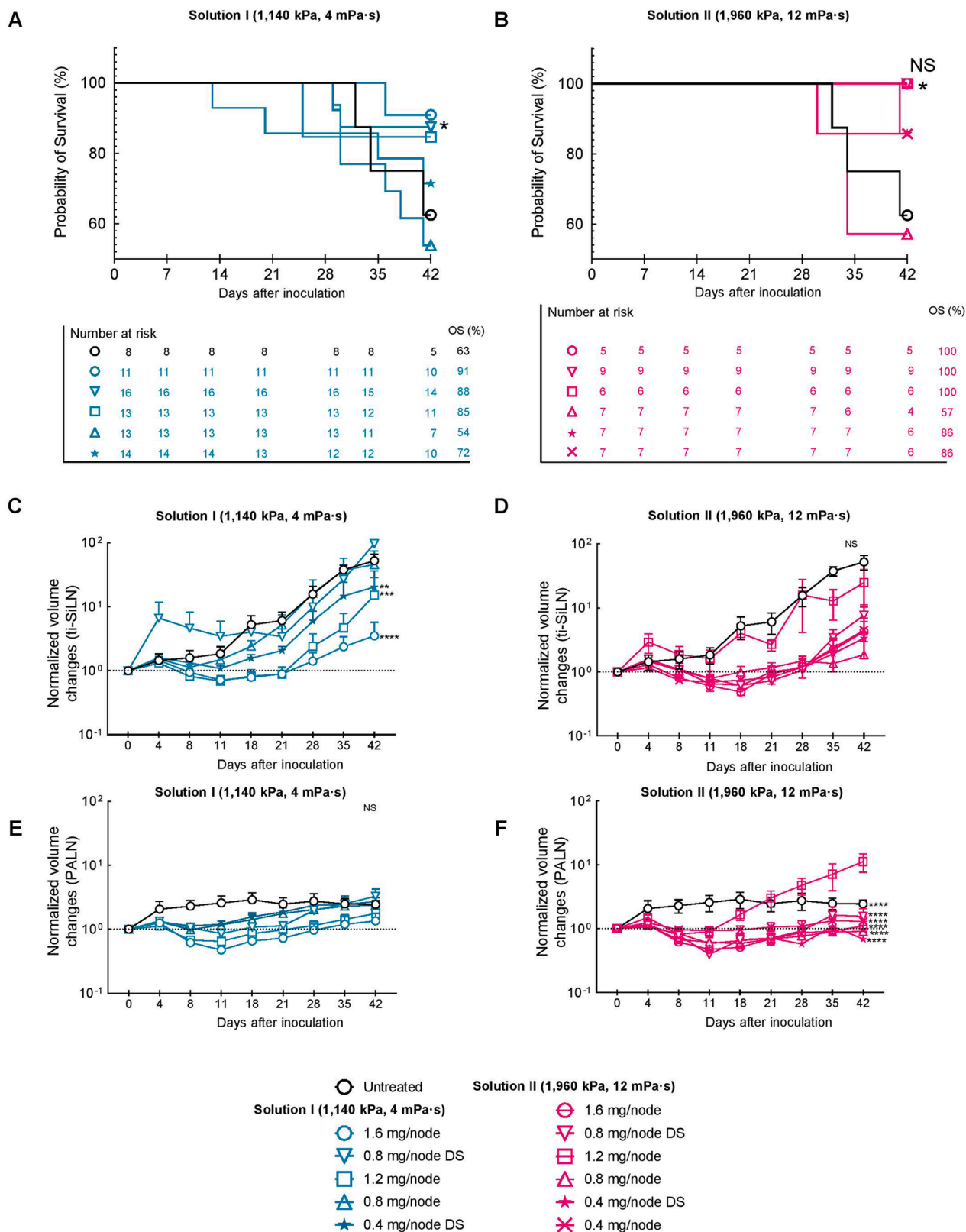
**Fig. 3.** Survival probability and volume change. A. Kaplan-Meier survival curves of mice treated by LDDS with solution I (1,140 mg, 4 mPa·s). Data are shown as the mean ± SEM (* $P \leq 0.05$, ** $P \leq 0.01$, *** $P \leq 0.001$, **** $P \leq 0.0001$). $n = 13 - 16$/group. B. Kaplan-Meier survival curves of mice treated by LDDS with solution II (1,960 mg, 12 mPa·s). Data are shown as the mean ± SEM (* $P \leq 0.05$, ** $P \leq 0.01$, *** $P \leq 0.001$, **** $P \leq 0.0001$). n = 4 – 9/group. C-F, Volume change in ti-SiLN or PALN, treated with solution I (1,140 mg, 4 mPa·s) or solution II (1,960 mg, 12 mPa·s). Untreated ($n = 8$); Solution I (1,140 kPa, 4 mPa·s). $n = 13–16$/group; Solution II (1,960 kPa, 12 mPa·s). $n = 4 – 9$/group. Data are shown as the mean ± SEM (* $P \leq 0.05$, ** $P \leq 0.01$, *** $P \leq 0.001$, **** $P \leq 0.0001$). C. Volume change in ti-SiLN, treated with solution I (1,140 mg, 4 mPa·s). D. Volume change in PALN, treated with solution I (1,140 mg, 4 mPa·s). E. Volume change in ti-SiLN, treated with solution II (1,960 mg, 12 mPa·s). F. Volume change in PALN, treated with solution II (1,960 mg, 12 mPa·s).

**Table 1**
Response criteria per group for overall survival.

| | Total | Partial response in the ti-SiLN | Partial response in the PALN | Complete response |
|---|---|---|---|---|
| Untreated | 8 (100%) | 0 (0%) | 0 (0%) | 0 (0%) |
| Solution I (1,140 kPa, 4 mPa·s) | | | | |
| 1.6 mg/node | 11 (100%) | 4 (40.0%) | 7 (70.0%) | 3 (30.0%) |
| 0.8 mg/node DS | 16 (100%) | 4 (28.6%) | 12 (85.7%) | 3 (21.4%) |
| 1.2 mg/node | 13 (100%) | 6 (54.5%) | 10 (90.9%) | 4 (36.4%) |
| 0.8 mg/node | 13 (100%) | 2 (28.6%) | 5 (71.4%) | 1 (14.3%) |
| 0.4 mg/node DS | 14 (100%) | 5 (50.0%) | 5 (50.0%) | 3 (30.0%) |
| Solution II (1,960 kPa, 12 mPa·s) | | | | |
| 1.6 mg/node | 5 (100%) | 1 (20.0%) | 2 (40.0%) | 0 (0.%) |
| 0.8 mg/node DS | 9 (100%) | 3 (33.3%) | 6 (66.7%) | 2 (22.2%) |
| 1.2 mg/node | 7 (100%) | 4 (57.1%) | 5 (71.4%) | 4 (57.1%) |
| 0.8 mg/node | 7 (100%) | 2 (66.7%) | 3 (75.0%) | 2 (50.0%) |
| 0.4 mg/node DS | 7 (100%) | 4 (66.7%) | 7 (100%) | 4 (66.7%) |
| 0.4 mg/node | 7 (100%) | 2 (33.3%) | 3 (50.0%) | 1 (16.7%) |

tumor infiltration in the PALN (Fig. 4C); representative images are shown in Fig. 5. Multi-foci tumors with associated necrosis were observed in the ti-SiLN and PALN of the untreated group. LN tissue was replaced by tumor and the pre-existing LN structure destroyed by tumor growth from the marginal sinus to the parenchyma (Fig. 5A). A small number of residual tumor cells was observed in the ti-SiLN, but no tumor cells were found in the PALN after treatment with 1.6 mg/node of Solution I (Fig. 5B). For the 1.6 mg/node treatment with Solution II, tumor cell proliferation was still seen in the marginal sinus and parenchyma of the LN, with necrosis in some areas in the ti-SiLN and the tumor mass was associated with necrosis in marginal sinus and parenchyma of the PALN (Fig. 5B). After a DS of 0.4 mg/node Solution I, tumor cell proliferation was found in the parenchyma and marginal sinus of the ti-SiLN, whereas no tumor cells were found in the PALN (Fig. 5C). No tumor cells were observed in the ti-SiLN and PALN after treatment with a DS of 0.4 mg/node Solution II (Fig. 5C). As result, at a SS of 1.6 mg/node, Solution I was shown to have a high antitumor effect and Solution II a low antitumor effect (Fig. 4C, Fig. 5B). After a DS of 0.4 mg/node, Solution II had a higher antitumor effect than Solution I (Fig. 4C, Fig. 5C). Metastases in the PALN disappeared after treatment with Solution B. In a comparison between Solution I and Solution II, Solution II clearly had a higher anti-tumor effect overall (Fig. 4C, Fig. 5). Response criteria for overall survivals are listed in Table 1; the highest PR and CR were found after treatment with the 1.2 mg/node of Solution I (36.4 % CR) and 0.4 mg/node DS of Solution II (66.7 %), respectively.

### 3.4. Dosage dependent immune shifting of LDDS-injected DTX

Next immune profiling was analyzed, after a SS or DS of LDDS-injected DTX, by checking the gene expression of immune cells in the ti-SiLN (Fig. 6A), PALN (Fig. 6B) and spleen (Fig. 6C). Pro-inflammatory cytokines were upregulated in the groups of ti-SiLN, PALN and spleen treated with DS compared to the SS groups. Therefore, tumor infiltration lymphocytes were increased in the above organs of the DS groups compared to the SS group. Tumor suppressors were upregulated in the DS groups compared to the SS group, excluding IL10 in the ti-SiLN of the DS groups. The levels of the cell death markers Hsp70, Hsp90 and CRT

were increased in the DS groups compared to the SS groups. Overall, IL6, IL12-α, IL12-β, IL10, Hsp90 and CRT levels were increased in ti-SiLN; CD4 and PDL1 expression were increased in PALN; and IFN-γ, TNF-α, IL10 and TGF-β were increased in the spleen of the SS groups compared with the controls (data not shown). For the DS groups, IL1b, and IL10 were decreased in the ti-SiLN; IL1-β, IL10 and CRT were decreased whereas all immune markers expression levels were enhanced in the PALN compared to the controls (data not shown).

### 3.5. Adverse events and side effects evaluation of LDDS-injected DTX dosage dependency

During the study, we did not observe any dermatological or gastrointestinal side effects, abnormalities, adverse events or unusual motor skills that could be attributed to the actions of DTX. To evaluate the presence of dosage-induced acute hepatic toxicity, blood was drawn from IVC 3 days after treatment with SS or DS of DTX at 1,960 kPa (12 mPa•s) compared with same from non-treated groups. For the baseline, we used histology confirmed healthy 12 week old MXH10/Mo/lpr mice for the hematological and biochemical tests. As described in Fig. 7A, RBC, WBC, Hgb, and HCT were 1-fold elevated in the untreated SS compared with baseline. For the DS groups, WBC, PLT and PCT were elevated compared to baseline and the untreated DS group. No changes were found in liver functions based on biochemical tests (Fig. 7B). There were no significant differences in body weight between the various groups, except for the group that received 1.6 mg/node (Solution I) (Supplementary Table S3).

### 3.6. Treatment evaluation of LDDS administered CDDP at different osmotic pressures and viscosities

To evaluate the flow pattern of anticancer drugs at different osmotic pressures and viscosities from tumor free LN, tumor cells were inoculated to the PALN, and CDDP was infused into the tumor free SiLN at a rate of 10 μL/min through the LDDS (Fig. 8A). The flow pattern of CDDP at 152 kPa to 3,641 kPa (1 - 262 mPa•s) showed a strong signal in the infusion side that was similar to the ti-SiLN injected DTX (Fig. 8B). Drug reachability into the ti-PALN was reduced with an increase in osmotic pressure and viscosity. However, interim edema around the region of the tumor free SiLN in the high viscosity groups (2,768 kPa 55 mPa•s and 3,641 kPa 262 mPa•s) 3 days after CDDP infusion (6 days after inoculation) was observed by naked eye observation and ultrasound imaging, but not in the low viscosity groups (Fig. 8B). Histopathology revealed that proliferation of tumor cells in the ti-PALN and excessive necrotic areas found in the SiLN were less than in the 1,024 kPa (2 mPa•s) group after the LDDS infusion (Fig. 8C, D). In the 1,897 kPa (12 mPa•s) group, no tumor cells were found in the ti-PALN, but necrotic foci were detected in the SiLN. In the 2,768 kPa 55 (mPa•s) and 3,641 kPa (262 mPa•s) groups, proliferation of tumor cells and mass were found in the ti-PALN and necrotic areas in the SiLN, with remarkable edema in the marginal sinus. Based on these results, we conclude that LDDS infusion of anticancer drugs at a low-rate filled the injection site of the LN, which migrated to the marginal sinus of the downstream LNs (Fig. 8E); in a solution <1,024 kPa (2 mPa•s) flow was upwards towards the systemic circulation. Interestingly, LDDS infused CDDP at 1,897 kPa (12 mPa•s) filled the injection site and its downstream LN resulting in greater tumor inhibition. Moreover, LDDS infused CDDP at greater than 2,768 kPa (55 mPa•s) filled the injection site, but did not flow throughout the lymphatic vessels.

### 4. Discussion

LDDS is an administration method to treat metastatic lymph nodes as well as metastatic lymph nodes downstream of the lymphatic network by delivering the drug directly to the metastatic lymph nodes [18]. It is one of alternative routes, such as topical, intranasal, subcutaneous and
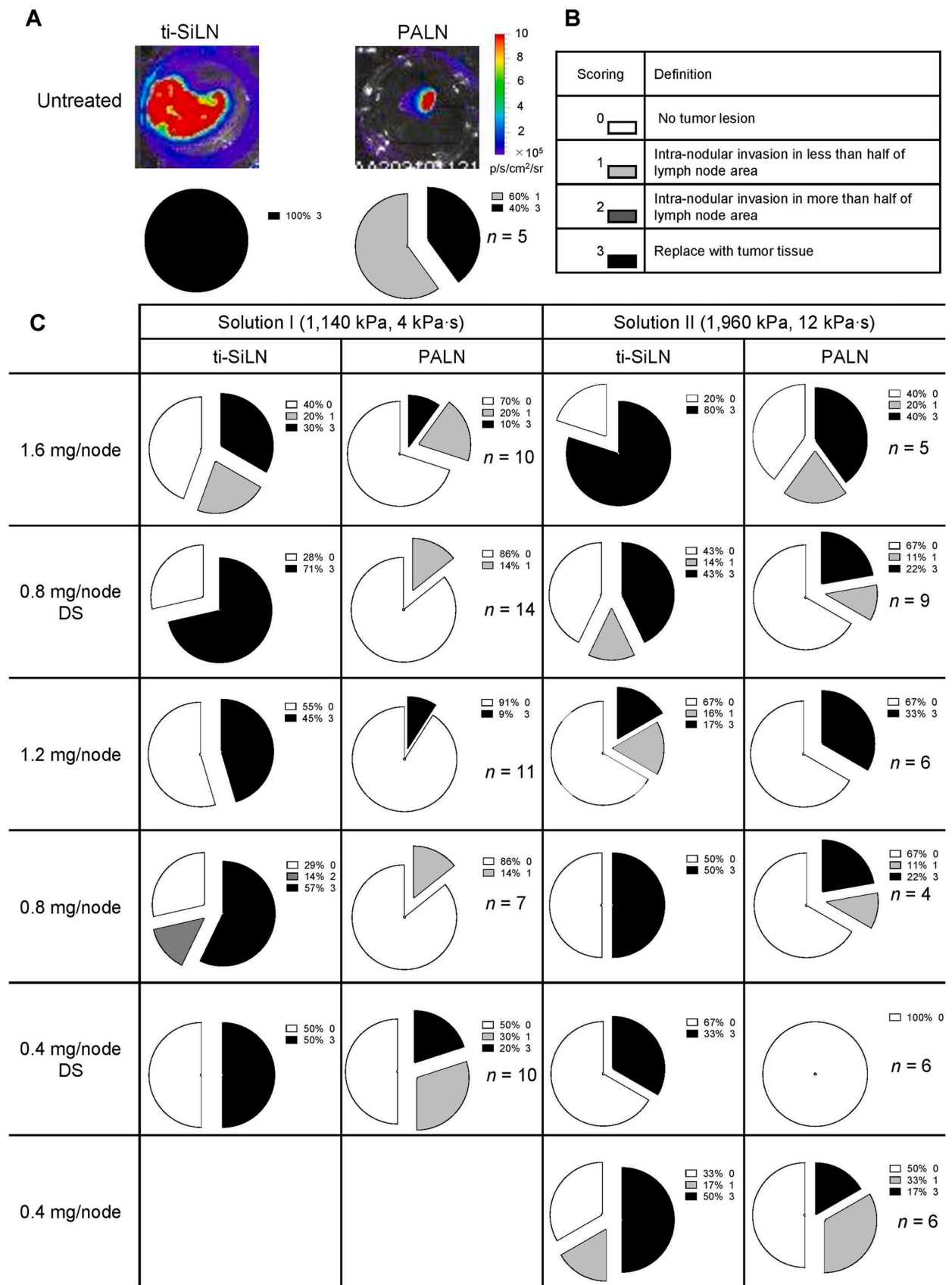
**Fig. 4.** Histological scoring in ti-SiLN and PALN on day 42. A. Untreated samples, $n = 5$ and representative *ex vivo* luminescence images for untreated sample. B. Design and validation of a histological scoring system for lymph node metastasis. C. Exploded pie chart showing histological scoring with different conditions.
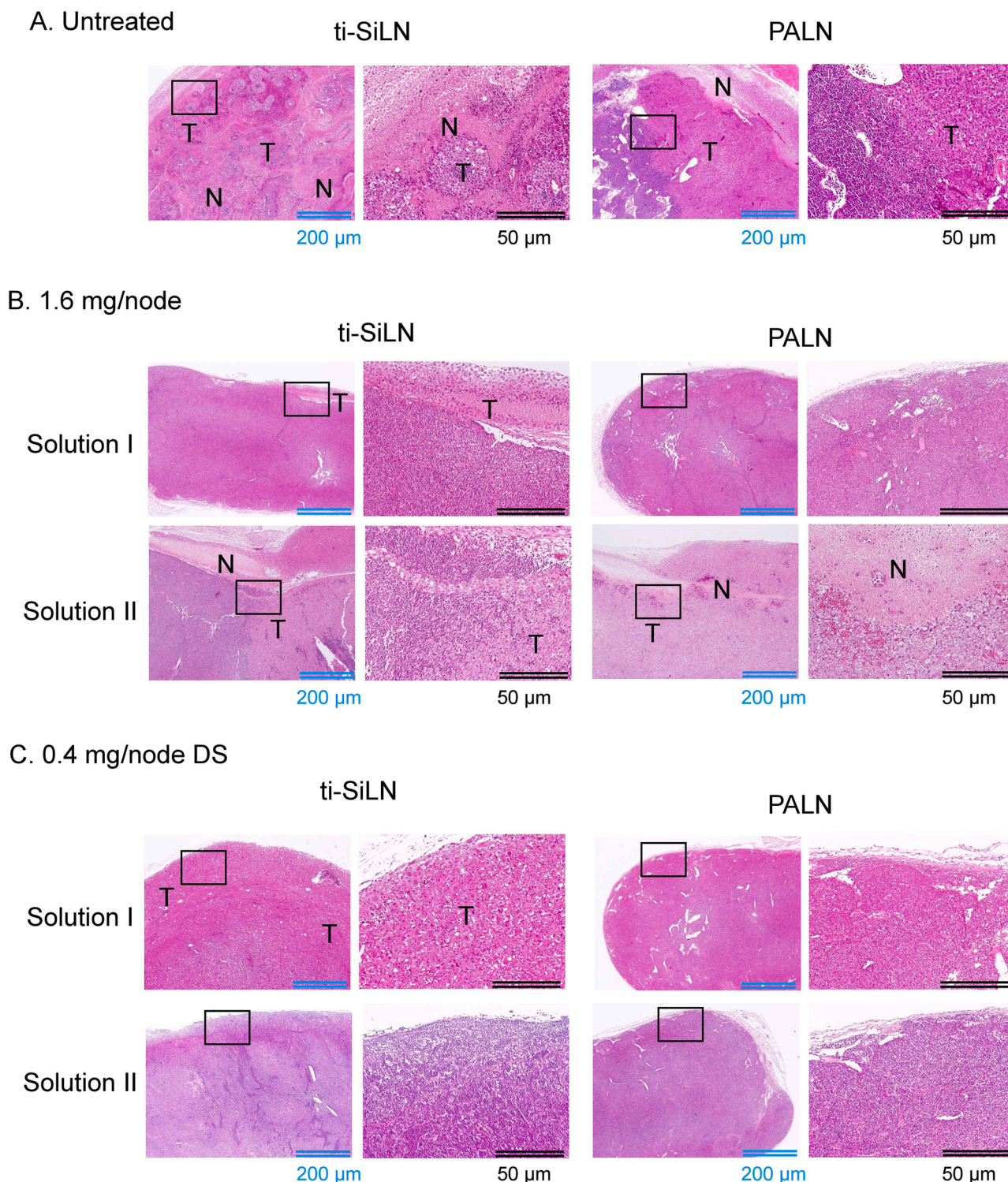
**Fig. 5.** Histopathological evaluation. Histopathological changes in the proper axillary lymph node (PALN) after DTX administration into ti-SiLN using the LDDS. The HE-stained sections on the right correspond to the regions indicated by rectangles in the HE-stained sections on the left. Scale bars: 50 μm (left) and 200 μm (right). T: tumor, N: necrosis.

intramuscular administration, where local toxicities limit the dosage. In the present study, MXH10/Mo/lpr mice were used and the dose of DTX varied per lymph node (0.4 mg, 0.8 mg, 1.2 mg, 1.6 mg) as a SS or DS to evaluate the long-term antitumor effects (Fig. 1, Fig. 2) and the survival rates (Fig. 3). In our previous study, we found that high osmotic pressure and viscosity solutions without any additive anticancer agents do not have an inhibitory effect on tumor; it dilates lymphatic vessels between

LNs and the marginal sinus of LN then increases reachability and flow of solution in the LNs [25,26,36]. The maximum recommended starting dose (MRSD) was verified. DTX was dissolved in solution I (1,140 kPa, 4 mPa·s) and solution II (1,960 kPa, 12 mPa·s). The MRSD depended on the osmotic pressure and viscosity of the solvent, the dose and the total dosage. For example, at a single dose of 1.6 mg/node, Solution I (1,140 kPa, 4 mPa•s) showed the highest antitumor effect, while Solution II (1,
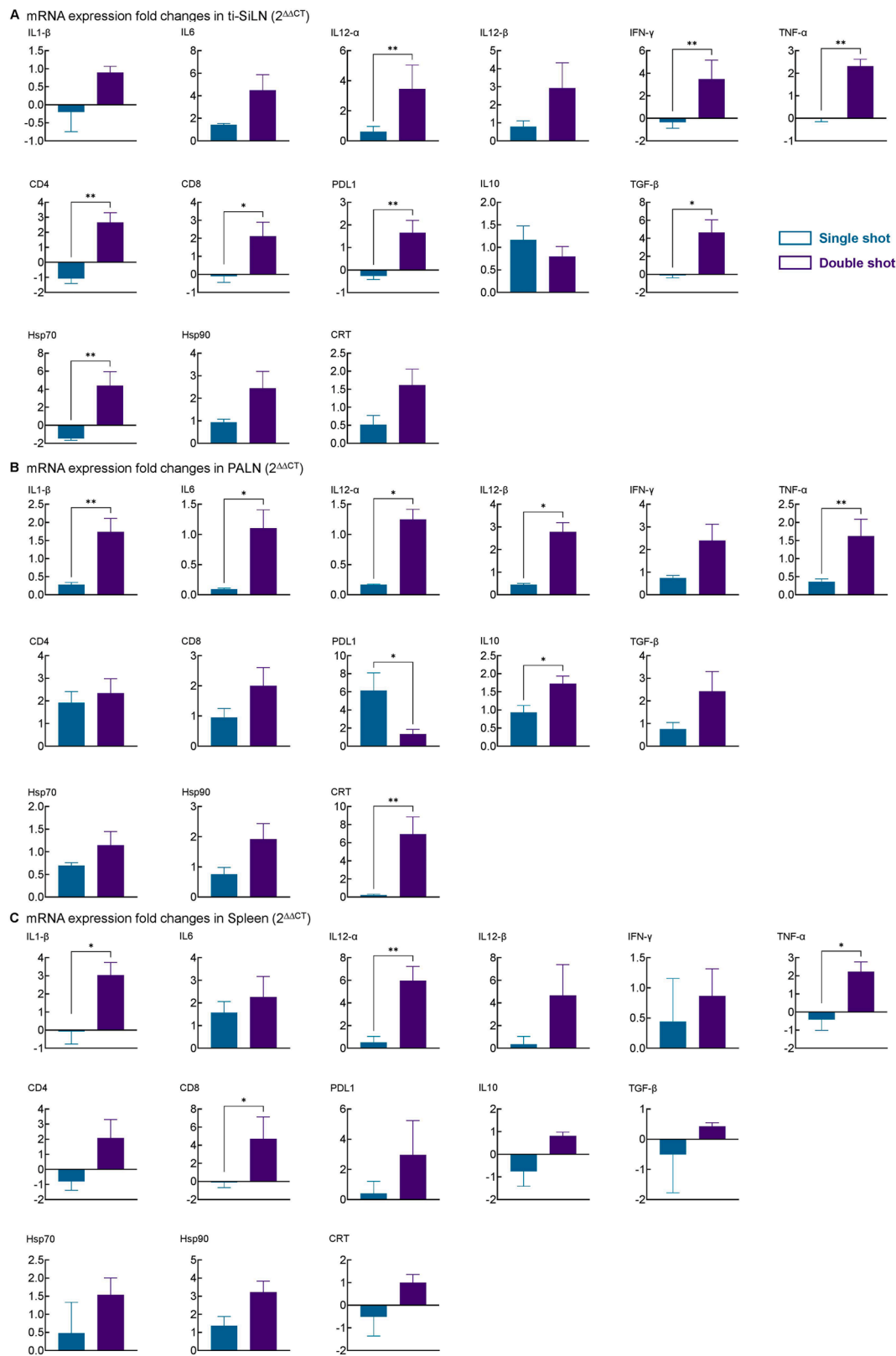
**Fig. 6.** Immune shifting of DTX dosage dependency (0.4 mg/node of Solution II). Spleen, ti-SiLN and PALN were harvested 3 days after treatment and immersed in RNA*later*, mRNA isolated and cDNA synthesized. Spleen, ti-SiLN, and PALN mRNA gene expression of the following markers, pro-inflammatory cytokines (IL1-β, IL6, IL12-α, IL12-β, IFN-γ and TNF-α), tumor infiltrating lymphocytes (CD4, CD8, and PDL1), tumor suppressor (IL10 and TGF-β), and immunogenic cell death (Hsp70, Hsp90 and calreticulin) was performed pre-designed primers by Integrated DNA. Data were normalized to internal control (GAPDH) of each sample, and untreated and treated samples were compared to the main relative gene expression. Data are presented as the mean ± SEM (* $P \leq 0.05$, ** $P \leq 0.01$, *** $P \leq 0.001$, **** $P \leq 0.0001$). A. Spleen. B. ti-SiLN. C. PALN.
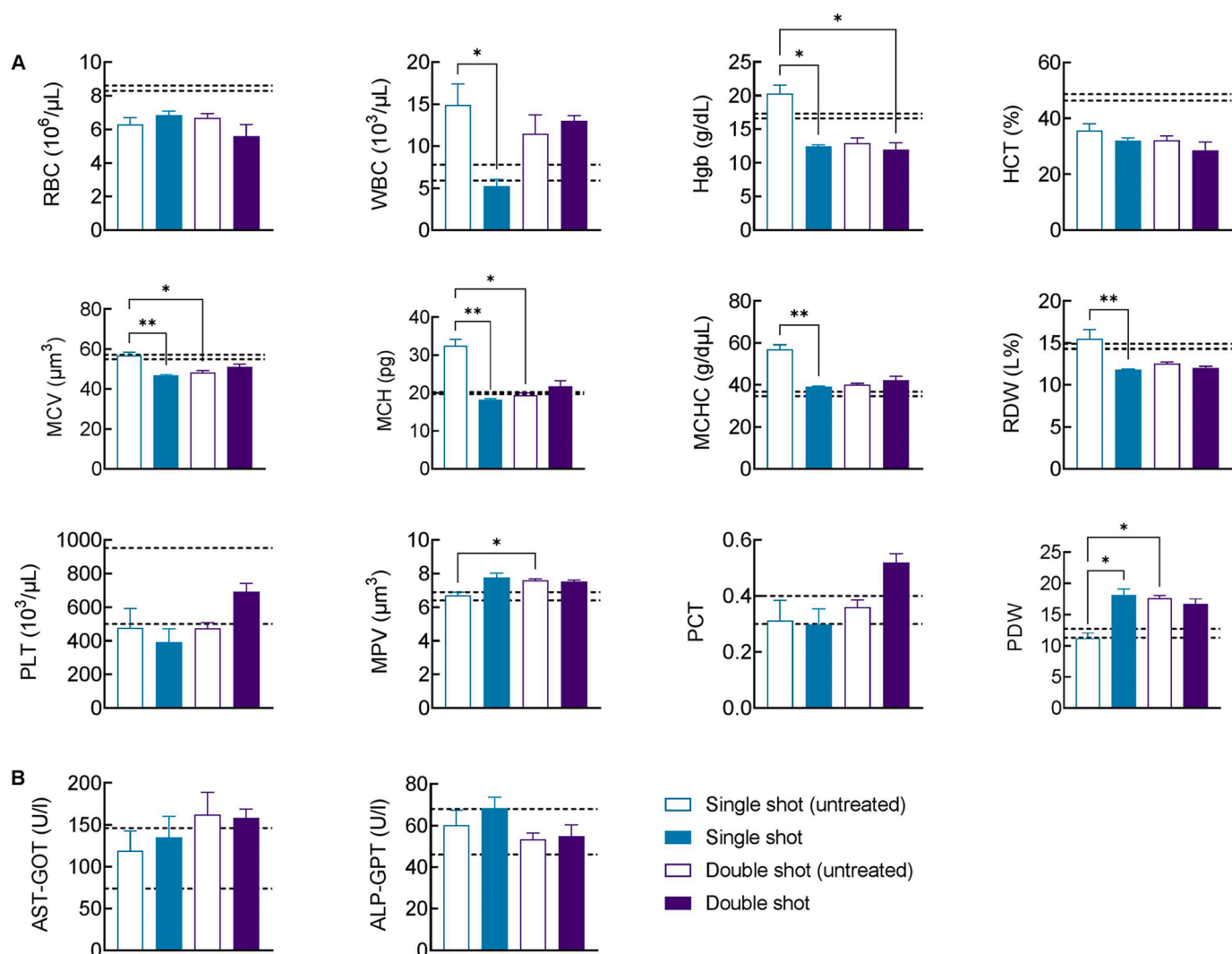
**Fig. 7.** Hematology and liver function tests. Blood harvested from IVC 3 days after treatment. Hematology and liver function tests were performed for screening of any adverse event or toxicity. Data presented in mean ± SEM (* $P \leq 0.05$, ** $P \leq 0.01$, *** $P \leq 0.001$, **** $P \leq 0.0001$).

960 kPa, 12 mPa•s) showed the lowest antitumor effect (Fig. 1, Fig. 2 and Table 1). At a DS of 0.4 mg/node DS, the antitumor effect of Solution II was higher than that of Solution I. In other words, the accumulation of high concentrations of DTX in ti-SiLNs may have resulted in necrosis of SiLN tissues, which in turn reduced the drug delivery capacity from ti-SiLNs to the PALNs, leading to the decreased therapeutic effect in the PALNs (Fig. 1, Fig. 2, Fig. 4 and Fig. 5). Administration of hyperosmotic fluid into the lymph node caused the lymphatic channels occluded by tumor cells to dilate due to the outflow of blood components from capillaries and high endothelial venules (HEV) in the parenchyma of the lymph node, while viscosity may be related to drug retention [25, 26]. Detailed studies on the flow dynamics of blood, interstitial fluid, and lymphatic fluid are required.

The clinical application of LDDS is best suited for the treatment of metastatic lymph nodes in head and neck or breast cancer, due to the ease of access to the lymph nodes. The head and neck region are one of the most frequent cancer sites, with approximately two-thirds of cancers being locally advanced (LA-HNC). Despite technological advances in radiation therapy (RT) and the development of bio-RT and new chemotherapy-RT combinations, about 40% of locally advanced cancers fail to respond or relapse after primary treatment [37]. Fifty to sixty percent of these patients develop locoregional recurrence within 2 years [38]. Metastasis in the regional lymph nodes occurs in about 30% of

head and neck cancer patients and the median survival is approximately 10 months. Therefore, control of lymph node metastasis alone will significantly improve survival.

In primary monotherapy for recurrent, unresectable or metastatic disease in head and neck cancer, DTX is administered i.v. at a concentration of 65 – 162 mg/body (40 – 100 mg/m²) per hour, followed by repeated doses every 3 weeks[39], where the human body weight was 60 kg and body surface area 1.62 m²[33]. Clinically, neutropenia occurs when DTX is administered at a dose of ≥ 50 mg/m² in the majority of patients treated [40]. Other side effects include hypersensitivity reactions (HSRs), neurotoxicity, cutaneous reactions, alopecia and asthenia [41]. In marked contrast, when DTX was administered using LDDS there were few adverse events.

The concentrations of DTX used in the experiments on mice were 0.4 – 1.6 mg/node, and assuming the same dose normalized between species, it is assumed that the same dose of DTX will be administered to human lymph nodes. This dose is 0.7 – 26 g/kg and 0.25 – 1.0 mg/m² for a 60 kg human with a surface area of 1.62 m². A simple calculation was made to convert current study doses into human equivalent dose (HED), and doses ranged from 30 mg/m² to 120 mg/m² (Table 2). With SS and DS treatment efficacy, toxicity and adverse events were reduced in LDDS injected DTX mice compared to clinical trials (Fig. 7). Moreover, LDDS administered DTX, 1.6 mg/node (120 mg/m²) of Solution I and 0.4 mg/
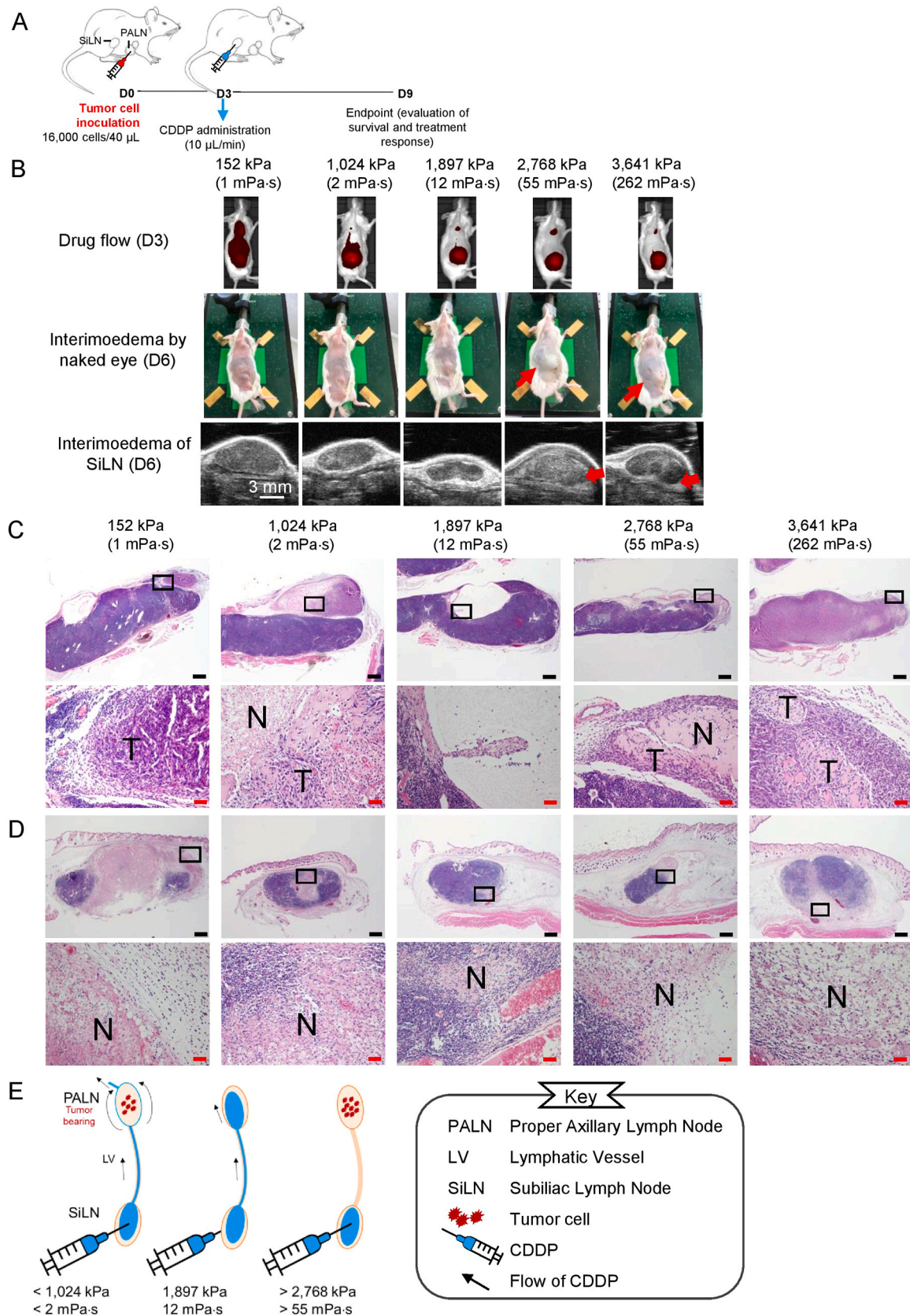
**Fig. 8.** Tumor inhibition of LDDS infused CDDP. A. Experimental design. B. Flow of CDDP at varied osmotic pressure and viscosity. Red arrow: edema. C. Histopathological evaluation of ti-PALN. Scale bar: black 500 μm; red: 200 μm; N, necrosis; T, tumor. D. Histopathological evaluation of SiLN. Scale bar: black 500 μm; red: 200 μm; N, necrosis; T, tumor. E. Flow dynamic of LDDS infused anticancer drugs.

**Table 2**
Dose conversion from mouse to human equivalent dose (HED).

| Drug concentration in mouse [mg/node] | Drug concentration in mouse [mg/kg]* | Converted drug concentration in human (HED) [mg/kg]** | Converted drug concentration in human [mg/m²] *** |
|---|---|---|---|
| 0.4 | 10 | 0.8 | 30 |
| 0.8 | 20 | 1.6 | 60 |
| 1.2 | 30 | 2.4 | 90 |
| 1.6 | 40 | 3.2 | 120 |

* Mouse bodyweight assumed to 40 g

** $ED\left(\frac{mg}{kg}\right) = Mouse\ \ dose\ \ \left(\frac{mg}{kg}\right) \times \frac{\text{Mouse}K_m}{\text{Human}K_m}$ where Mouse $K_m = 3$ and Human $K_m = 37$

*** $ED\left(\frac{mg}{m^2}\right) = \frac{HED\ \ \left(\frac{mg}{kg}\right) \times Weight(kg)}{0.007184 \times Height^{0.725} \times Weight^{0.425}}$ where Weight $= 60$ kg and Height $= 1.6$ m

node (30 mg/m²) DS of Solution II resulted in increased survival with superior antitumor effects (treatment response) and minimized adverse events. We identified 28 clinical trials (mono- or multicentered), that had used/were using DTX with interventions using other chemotherapeutic drugs or radiation, in the Clinicaltrials.gov database using the keywords "docetaxel", "lymph node" and "adult", irrespective of the primary tumor and disease condition. The data is summarized in Supplementary Table S4, excluding the following: terminated (1); status unknown (4); or IHC based evaluation (1). These clinical trials used 2 to 6 cycles of 60 – 100 mg/m² DTX, with intervention of other chemotherapy drugs or radiation or surgery, and overall survival with complete responses were recorded. While the systemic administration dose of DTX was about 100 mg to treat and prevent metastasis to distant organs including lymph nodes, LDDS administers only about 1/100th of this drug dose to the lymph nodes. Therefore, it can be safely assumed that most of the systemic side effects associated with the systemic administration of DTX will be negligible.

An increase of IL10 levels in the central immune system, PALN and ti-SiLN (Fig. 6) promotes CD4 T cell activation and proliferation, which in turn encourages the release of IFN-γ, and causes tumor cell death through cell mediated immune responses. Increase in proinflammatory cytokines such as IL1-β, IL6 and IL12 and TNF-α may cause interim edema as a result of intranodal injection of DTX; a further detailed investigation is needed.

Nevertheless, this early upregulation indicates that T lymphocytes in the DTX injected LN (ti-SiLN), its downstream LN (PALN) and splenic immune populations are orchestrators of cancer metastasis-inflammation interactions facilitating the improvement of survival and antitumor progression.

We evaluated the effectiveness of inhibiting the growth of tumors in the lymphatic system using anticancer drugs administered through the LDDS by treating metastatic LN (PALN) from its upstream LN (SiLN). We used CDDP and found that fluorescent signals were similar in different osmotic pressure and viscosity solutions, regardless of the drug class (Figs. 1 and 8). However, low osmotic pressure and viscosity solutions could not inhibit tumor growth in the ti-PALNs, resulting in a higher area of necrosis at the injection side (SiLN). We also observed that solutions with more than 2,700 kPa with 40 mPa•s were unable to suppress tumor growth in the ti-PALNs and induced edema in the marginal sinus of the injection site (SiLN) with necrosis in the LNs. We believe that the flow of drugs through the lymphatic vessel changed to the marginal sinus of the PALN when low osmotic pressure and viscosity solutions were injected at a low rate into the PALN. Moreover, solutions with high osmotic pressure and viscosity could not flow via the lymphatic vessel to its downstream LNs, causing edema. We concluded that the optimal range of osmotic pressure and viscosity solutions plays a crucial role in

delivering drugs to LNs and improving tumor inhibition in the lymphatic system after a chemotherapy dose (Fig. 8).

## 5. Conclusions

The author's group has obtained approval from the Japanese Pharmaceuticals and Medical Devices Agency to conduct a phase 1 clinical trial using DTX given through the LDDS for the treatment of head and neck cancer, but the key point for the approval was the low dosage of DTX to be used compared with existing systemic administration of drugs. In order successfully to complete the clinical trial, it will be necessary to investigate the MRSD of DTX based on the parameters of osmotic pressure and viscosity of the solvent, frequency of administration, dose, pharmacokinetics, and physiological time to increase the survival rate and the long-term response rate to metastatic lymph nodes. From a safety perspective, LDDS administered low-concentration DTX without combining any anticancer treatments into the LNs and may be a novel approach for cancer management of cancerous LNs. We emphasize that LDDS is a groundbreaking method of delivering anticancer drugs specifically to cancer susceptible LNs and is designed to enhance the effectiveness of cancer treatment while minimizing side effects.

## Ethics statement

Approval of the research protocol by an Institutional Reviewer Board: Approval obtained from the Institutional Animal Care and Use Committee of Tohoku University (2019BeA-017–05/2018BeLMO-002–09) - Animal Studies: he guidelines of the Institutional Animal Care and Use Committee of Tohoku University were complied with for all investigations carried out using murine models including the ARRIVE protocol.

## Consent to participate

Not applicable.

## Consent for publication

Not applicable.

## CRediT authorship contribution statement

**Kodama Tetsuya:** Conceptualization, Funding acquisition, Methodology, Supervision, Writing – original draft, Writing – review & editing. **Mori Shiro:** Formal analysis, Writing – original draft, Writing – review & editing. **Sugiura Tsuyoshi:** Supervision. **Sukhbaatar Ariunbuyan:** Data curation, Formal analysis, Funding acquisition, Investigation, Methodology, Project administration, Validation, Visualization, Writing – original draft, Writing – review & editing.

## Declaration of Competing Interest

The authors declare that they have no competing interests.

## Data Availability

Data will be made available on request.

## Acknowledgment

## Appendix A. Supporting information

Supplementary data associated with this article can be found in the online version at doi:10.1016/j.biopha.2023.116085.

## References

[1] D.E. Johnson, B. Burtness, C.R. Leemans, V.W.Y. Lui, J.E. Bauman, J.R. Grandis, Head and neck squamous cell carcinoma, Nat. Rev. Dis. Prim. 6 (1) (2020) 92.

[2] A. Sukhbaatar, S. Mori, Y. Saiki, T. Takahashi, A. Horii, T. Kodama, Lymph node resection induces the activation of tumor cells in the lungs, Cancer Sci. 110 (2) (2019) 509–518.

[3] A. Sukhbaatar, M. Sakamoto, S. Mori, T. Kodama, Analysis of tumor vascularization in a mouse model of metastatic lung cancer, Sci. Rep. 9 (1) (2019) 16029.

[4] J. Zheng, L. Jia, S. Mori, T. Kodama, Evaluation of metastatic niches in distant organs after surgical removal of tumor-bearing lymph nodes, BMC Cancer 18 (1) (2018) 608.

[5] S. Jalkanen, M. Salmi, Lymphatic endothelial cells of the lymph node, Nat. Rev. Immunol. 20 (9) (2020) 566–578.

[6] M. Jafarnejad, A.Z. Ismail, D. Duarte, C. Vyas, A. Ghahramani, D.C. Zawieja, C. Lo Celso, G. Poologasundarampillai, J.E. Moore Jr., Quantification of the whole lymph node vasculature based on tomography of the vessel corrosion casts, Sci. Rep. 9 (1) (2019) 13380.

[7] I.D. Kelch, G. Bogle, G.B. Sands, A.R.J. Phillips, I.J. Legrice, P.R. Dunbar, High-resolution 3D imaging and topological mapping of the lymph node conduit system, PLOS Biol. 17 (12) (2019) e3000486.

[8] T. Kodama, S. Mori, M. Nose, Tumor cell invasion from the marginal sinus into extranodal veins during early-stage lymph node metastasis can be a starting point for hematogenous metastasis, J. Cancer Metastas-.-. Treat. 4 (11) (2018) 56.

[9] T. Yamaki, A. Sukhbaatar, R. Mishra, R. Kikuchi, M. Sakamoto, S. Mori, T. Kodama, Characterizing perfusion defects in metastatic lymph nodes at an early stage using high-frequency ultrasound and micro-CT imaging, Clin. Exp. Metastas. (2021).

[10] K. Takeda, S. Mori, T. Kodama, Study of fluid dynamics reveals direct communications between lymphatic vessels and venous blood vessels at lymph nodes of mice, J. Immunol. Methods 445 (2017) 1–9.

[11] L. Shao, K. Takeda, S. Kato, S. Mori, T. Kodama, Communication between lymphatic and venous systems in mice, J. Immunol. Methods 424 (2015) 100–105.

[12] E.R. Pereira, D. Kedrin, G. Seano, O. Gautier, E.F.J. Meijer, D. Jones, S.M. Chin, S. Kitahara, E.M. Bouta, J. Chang, E. Beech, H.S. Jeong, M.C. Carroll, A.G. Taghian, T.P. Padera, Lymph node metastases can invade local blood vessels, exit the node, and colonize distant organs in mice, Science 359 (6382) (2018) 1403–1407.

[13] H.S. Jeong, D. Jones, S. Liao, D.A. Wattson, C.H. Cui, D.G. Duda, C.G. Willett, R. K. Jain, T.P. Padera, Investigation of the lack of angiogenesis in the formation of lymph node metastases, J. Natl. Cancer Inst. 107 (9) (2015).

[14] M. Mikada, A. Sukhbaatar, Y. Miura, S. Horie, M. Sakamoto, S. Mori, T. Kodama, Evaluation of the enhanced permeability and retention effect in the early stages of lymph node metastasis, Cancer Sci. 108 (5) (2017) 846–852.

[15] L. Li, S. Mori, M. Kodama, M. Sakamoto, S. Takahashi, T. Kodama, Enhanced sonographic imaging to diagnose lymph node metastasis: importance of blood vessel volume and density, Cancer Res. 73 (7) (2013) 2082–2092.

[16] L. Li, S. Mori, M. Sakamoto, S. Takahashi, T. Kodama, Mouse model of lymph node metastasis via afferent lymphatic vessels for development of imaging modalities, PloS One 8 (2) (2013) e55797.

[17] S. Kato, K. Takeda, A. Sukhbaatar, M. Sakamoto, S. Mori, K. Shiga, T. Kodama, Intranodal pressure of a metastatic lymph node reflects the response to lymphatic drug delivery system, Cancer Sci. 111 (11) (2020) 4232–4241.

[18] Y. Miura, M. Mikada, T. Ouchi, S. Horie, K. Takeda, T. Yamaki, M. Sakamoto, S. Mori, T. Kodama, Early diagnosis of lymph node metastasis: importance of intranodal pressures, Cancer Sci. 107 (3) (2016) 224–232.

[19] R. Omranipour, B. Eslami, M. Vasigh, H. Mahmoodzadeh, M. Shirkhoda, M. A. Mohagheghi, A. Jalaeefar, Axillary intranodal pressure measurement: a complementary technique for detection of lymph node metastasis in breast cancer patients, Clin. Cancer Invest. J. 9 (2) (2020) 49.

[20] N.L. Trevaskis, L.M. Kaminskas, C.J. Porter, From sewer to saviour - targeting the lymphatic system to promote drug exposure and activity, Nat. Rev. Drug Discov. 14 (11) (2015) 781–803.

[21] T. Kodama, D. Matsuki, A. Tada, K. Takeda, S. Mori, New concept for the prevention and treatment of metastatic lymph nodes using chemotherapy administered via the lymphatic network, Sci. Rep. 6 (2016) 32506.

[22] S. Kato, Y. Shirai, C. Motozono, H. Kanzaki, S. Mori, T. Kodama, In vivo delivery of an exogenous molecule into murine T lymphocytes using a lymphatic drug delivery system combined with sonoporation, Biochem. Biophys. Res. Commun. 525 (4) (2020) 1025–1031.

[23] S. Kato, Y. Shirai, M. Sakamoto, S. Mori, T. Kodama, Use of a lymphatic drug delivery system and sonoporation to target malignant metastatic breast cancer cells proliferating in the marginal sinuses, Sci. Rep. -Uk 9 (2019).

[24] H. Fujii, S. Horie, A. Sukhbaatar, R. Mishra, M. Sakamoto, S. Mori, T. Kodama, Treatment of false-negative metastatic lymph nodes by a lymphatic drug delivery system with 5-fluorouracil, Cancer Med. 8 (5) (2019) 2241–2251.

[25] A. Sukhbaatar, S. Mori, T. Kodama, Intranodal delivery of modified docetaxel: Innovative therapeutic method to inhibit tumor cell growth in lymph nodes, Cancer Sci. (2022).

[26] R. Fukumura, A. Sukhbaatar, R. Mishra, M. Sakamoto, S. Mori, T. Kodama, Study of the physicochemical properties of drugs suitable for administration using a lymphatic drug delivery system, Cancer Sci. 112 (5) (2021) 1735–1745.

[27] H. Kim, H. Han, M. Jeong, J. Han, J.H. Park, Management of lymph node metastasis via local chemotherapy can prevent distant metastasis and improve survival in mice, J. Control Release 329 (2021) 847–857.

[28] K. Nagai, T. Sato, C. Kojima, Design of a dendrimer with a matrix metalloproteinase-responsive fluorescence probe and a tumor-homing peptide for metastatic tumor cell imaging in the lymph node, Bioorg. Med. Chem. Lett. 33 (2021) 127726.

[29] J. Ge, L. Chen, B. Huang, Y. Gao, D. Zhou, Y. Zhou, C. Chen, L. Wen, Q. Li, J. Zeng, Z. Zhong, M. Gao, Anchoring group-mediated radiolabeling of inorganic nanoparticles horizontal line a universal method for constructing nuclear medicine imaging nanoprobes, ACS Appl. Mater. Interfaces 14 (7) (2022) 8838–8846.

[30] T. Ouchi, A. Sukhbaatar, S. Horie, M. Sakamoto, S. Mori, T. Kodama, Superselective drug delivery using doxorubicin-encapsulated liposomes and ultrasound in a mouse model of lung metastasis activation, Ultrasound Med. Biol. 44 (8) (2018) 1818–1827.

[31] A.B. Nair, S. Jacob, A simple practice guide for dose conversion between animals and human, J. Basic Clin. Pharm. 7 (2) (2016) 27–31.

[32] Food and Drug Administration, Estimating the maximum safe starting dose in initial clinical trials for therapeutics in adult healthy volunteers, in: O.o.N.D.i.t.C.f. D.E.a.R. (CDER) (Ed.) Rockville, MD, 2005.

[33] M.J. Saadh, M. Haddad, M.F. Dababneh, M.F. Bayan, B.A. Al-Jaidi, A guide for estimating the maximum safe starting dose and conversion it between animals and humans, Syst. Rev. Pharm. 11 (8) (2020) 98–101.

[34] L. Shao, S. Mori, Y. Yagishita, T. Okuno, Y. Hatakeyama, T. Sato, T. Kodama, Lymphatic mapping of mice with systemic lymphoproliferative disorder: usefulness as an inter-lymph node metastasis model of cancer, J. Immunol. Methods 389 (1-2) (2013) 69–78.

[35] R. Kikuchi, A. Sukhbaatar, M. Sakamoto, S. Mori, T. Kodama, A model system for studying superselective radiotherapy of lymph node metastasis in mice with swollen lymph nodes, Clin. Transl. Radiat. Oncol. 20 (2020) 53–57.

[36] R. Mishra, A. Sukhbaatar, A. Dorai, S. Mori, K. Shiga, T. Kodama, Drug formulation augments the therapeutic response of carboplatin administered through a lymphatic drug delivery system, Cancer Sci. 114 (1) (2023) 259–270.

[37] P. Pisani, M. Airoldi, A. Allais, P. Aluffi Valletti, M. Battista, M. Benazzo, R. Briatore, S. Cacciola, S. Cocuzza, A. Colombo, B. Conti, A. Costanzo, L. Della Vecchia, N. Denaro, C. Fantozzi, D. Galizia, M. Garzaro, I. Genta, G.A. Iasi, M. Krengli, V. Landolfo, G.V. Lanza, M. Magnano, M. Mancuso, R. Maroldi, L. Masini, M.C. Merlano, M. Piemonte, S. Pisani, A. Prina-Mello, L. Prioglio, M. G. Rugiu, F. Scasso, A. Serra, G. Valente, M. Zannetti, A. Zigliani, Metastatic disease in head & neck oncology, Acta Otorhinolaryngol. Ital. 40 (Suppl. 1) (2020) S1–S86.

[38] K. Shiga, T. Ogawa, T. Kobayashi, S. Ueda, A. Kondo, A. Nanba, S. Kuwashima, Y. Asada, S. Suzuki, T. Nagahashi, M. Takahashi, M. Suzuki, A. Ishida, K. Watanabe, Y. Harabuchi, T. Himi, H. Sinkawa, H. Sato, S. Saijo, S. Fukuda, K. Tanaka, K. Ishikawa, K. Omori, M. Aoyagi, S. Hashimoto, Malignant melanoma of the head and neck: a multi-institutional retrospective analysis of cases in northern Japan, Head. Neck 34 (11) (2012) 1537–1541.

[39] The National Comprehensive Cancer Network, Head and neck cancer treatment regimens, (2018).

[40] E. Van Den Neste, D. de Valeriola, J. Kerger, H. Bleiberg, Z. Kusenda, C. Brassinne, S. Bartholomeus, J. Selleslags, P. Hennebert, H. Wythouck, I. Cazenave, F. Lefresne-Soulas, M. Piccart, A phase I and pharmacokinetic study of docetaxel administered in combination with continuous intravenous infusion of 5-fluoro-uracil in patients with advanced solid tumors, Clin. Cancer Res. 6 (1) (2000) 64–71.

[41] J.E. Cortes, R. Pazdur, Docetaxel, J. Clin. Oncol. 13 (10) (1995) 2643–2655.